Recent Advances in Spray Combustion: Spray Combustion Measurements and Model Simulation

Volume II

Edited by
Kenneth K. Kuo
Pennsylvania State University
University Park, Pennsylvania

Volume 171
PROGRESS IN
ASTRONAUTICS AND AERONAUTICS

Paul Zarchan, Editor-in-Chief
Charles Stark Draper Laboratory, Inc.
Cambridge, Massachusetts

Published by the
American Institute of Aeronautics and Astronautics, Inc.
1801 Alexander Bell Drive, Reston, Virginia 22091

ISBN 1-56347-181-7

Chapter 2

Behavior of Droplets in Pressure-Atomized Fuel Sprays with Coflowing Air Swirl

C. Presser*
National Institute of Standards and Technology, Gaithersburg, Maryland 20899
C. T. Avedisian†
Cornell University, Ithaca, New York 14853
J. T. Hodges‡
National Institute of Standards and Technology, Gaithersburg, Maryland 20899
and
A. K. Gupta§
University of Maryland, College Park, Maryland 20742

I. Introduction

SPRAY flames are commonly stabilized by using swirl burners or a variety of other mechanisms to establish a stable flame by recirculation of combustion gases and fuel vapors. Swirl burners have attracted considerable interest in recent years because of their ability to improve combustion efficiency and reduce the emission of pollutants in the waste disposal and power generation industries. The aerothermochemistry of swirl-stabilized flames is partly dependent on the degree of mixing between the fuel droplets and coflowing air stream that, in turn, is determined by the droplet transport and gas stream turbulence. The importance of matching the fuel spray pattern with the associated aerodynamic flowfield has been recognized through the direct application of laser sheet photography. Studies have shown that droplets pass through the flame sheet relatively unburnt when commercially available atomizers are used.[1] The effect of liquid penetration through the recirculation zone of swirl-stabilized spray flames leads to changes in flame structure and stability.[2] Information dealing with the effect of the gas

*Group Leader, Chemical Science and Technology Laboratory. Associate Fellow AIAA.
†Professor, Sibley School of Mechanical and Aerospace Engineering. Associate Fellow AIAA.
‡Research Engineer, Chemical Science and Technology Laboratory.
§Professor, Department of Mechanical Engineering. Fellow AIAA.

flowfield (both mean and fluctuating quantities) on the drag and trajectory of individual droplets of various sizes is critical for determining the dispersion of droplets within the surrounding airstream.

Several studies have focused on the effect of fuel spray pattern[3] and combustion air swirl[4–9] on the structure of spray flames. Owen[10] has carried out spray flame measurements using laser velocimetry (LV). Larger fuel droplets were found to be transported along the spray cone with velocities determined initially by the fuel nozzle characteristics. For droplets with large inertia relative to the turbulence, it was found that the initial conditions and early droplet displacement history dictate the dispersion of droplets farther downstream.[11] Unlike larger droplets, the smaller droplets lose their inertia and respond relatively quickly to the ambient gas velocity. The inertia of the larger droplets enables them to penetrate through the airstream with little interaction. For the smaller droplets, significant droplet velocity fluctuations about the mean occur as a result of their interaction with the airflow.

Large-scale motion of the flowfield plays a key role in the turbulent mixing processes, energy release, and pollutants emission.[12] The size, strength, and turbulence levels of the recirculation zone are important for affecting droplet transport.[13–15] It is apparent that increased levels of turbulence enhance droplet/air mixing, and thus promote near-stoichiometric combustion and flame stability, and reduce pollutant formation processes.

The effect of turbulence on droplet dispersion can be investigated using phase Doppler interferometry (PDI)[16] in different droplet-laden environments. The effect of operating parameters of the phase Doppler system on the mean and fluctuating velocities has been investigated.[17,18] In a previous paper by Presser and Gupta,[19] droplet size and velocity distributions were obtained using PDI in a nonswirling nonburning spray to examine shear layer effects near the spray boundary on droplet transport.

This paper examines droplet transport in a swirling kerosene spray using PDI. Droplet mean properties (namely, diameter, number density, and velocity) were measured to characterize the global features of the spray, whereas size and velocity distributions provided a more detailed picture of the behavior of individual droplets. Also, measured droplet velocity components were used to determine the direction of droplet motion throughout the spray from which conclusions are drawn concerning droplet transport. The results are compared with data for a nonswirling kerosene spray[19] for the same conditions of fuel and airflow rates to assess the influence of swirl on droplet transport.

Data are presented at several locations in the spray. Locations are chosen where gas recirculation near the nozzle results in significant droplet dispersion (i.e., near the central region of the spray) and where the droplet concentration is relatively high (i.e., near the spray boundary). In the latter case, larger size droplets are transported in a ballistic fashion, as their motion is not influenced strongly by the surrounding airflow pattern.

II. Experimental Apparatus

Experiments were carried out in a spray combustion facility that has been described elsewhere.[4,20] The facility includes a swirl burner with a movable 12-vane swirl cascade (see Fig. 1). The vanes rotate simultaneously to impart the desired

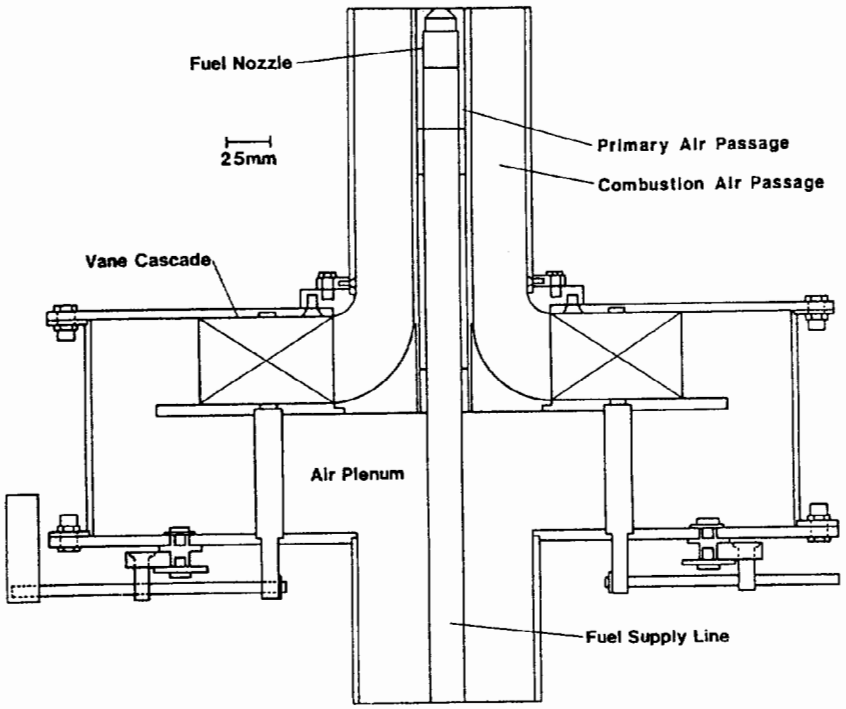

Fig. 1 Schematic of the movable-vane swirl burner.

degree of swirl intensity to the airstream that surrounds the fuel nozzle. The swirl number S refers to the ratio of the axial fluxes of angular momentum to linear momentum; the nominal value of S at the burner exit is calculated from theory developed for guide-vane cascades.[21] Experiments were carried out for swirling ($S = 0.53$) and nonswirling ($S = 0$) airstreams under nonburning conditions.[19] The value of $S = 0.53$ was chosen because of the good flame stability that is provided under burning conditions. A propane-fueled ring, located at approximately 300 mm downstream of the nozzle exit, was used as an afterburner to burn the droplets before they were exhausted to the atmosphere.

A simplex pressure-jet fuel nozzle was located along the centerline of the burner (at the burner exit). The fuel nozzle was operated at total air and fuel flow rates of 64.3 kg/h and 3.2 kg/h, respectively; these flow rates provided an input equivalence ratio of approximately 0.7. The nozzle generates a nominal 60-deg (full-angle) hollow-cone kerosene spray under unconfined conditions that is injected vertically upwards from the nozzle. A schematic of the hollow-cone spray, which includes the measurement grid, is illustrated in Fig. 2. In this study, measurements were obtained at axial positions of 10, 25.4, 50.8, and 76.2 mm. For each axial station, data were recorded in increments of 2.54 mm across the profile (at $z = 10$ mm the increment was 1.27 mm). Also shown are coordinates for several specific locations (designated L1–L5) where results are discussed in more detail. Locations L1, L2, and L4 are representative of the central region of the spray where recirculation

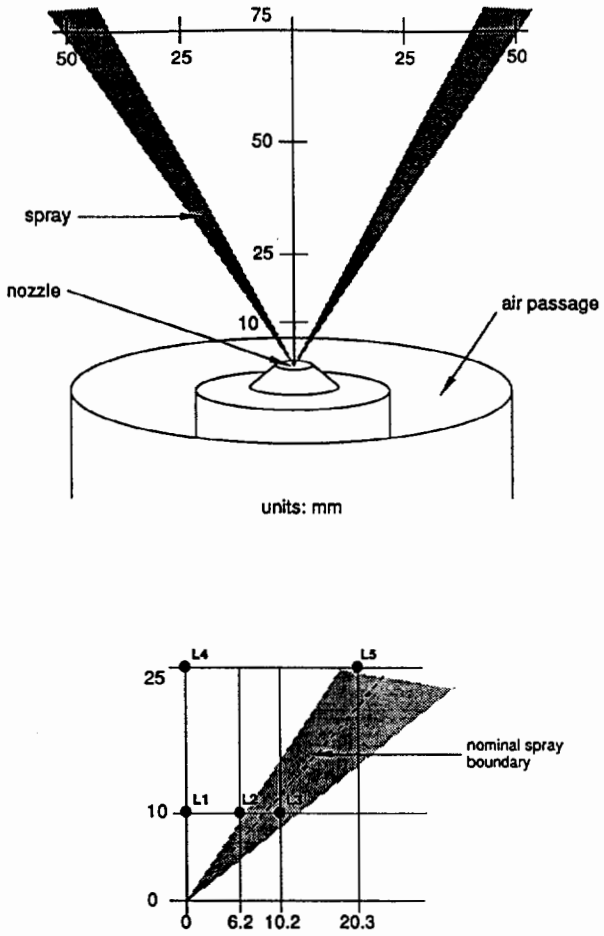

Fig. 2 Schematic of the spray boundary position; the numbers identify particular locations where the flow parameters are discussed in detail.

of the surrounding gases and droplet entrainment is expected to be significant. Locations L3 and L5 correspond to the spray boundary.

A stepper-motor-driven, three-dimensional traversing arrangement translates the burner assembly in the vertical and horizontal directions (see Fig. 3). All optical diagnostics are fixed in position about the burner assembly, and the burner translates independently of the optical equipment. Enough symmetry is assumed to exist about the spray axis so that measurements of spray properties in any particular plane containing that axis are considered representative of the entire spray. Measurements are reported in the plane in which the burner is traversed (X in Fig. 3). Additional details can be found elsewhere.[4,20]

The air flowfield was determined in a previous study,[4] using a single-component laser velocimetry system. Under swirling conditions, the mean axial air velocity is of the Rankine vortex type across the coflowing air passage at the burner exit

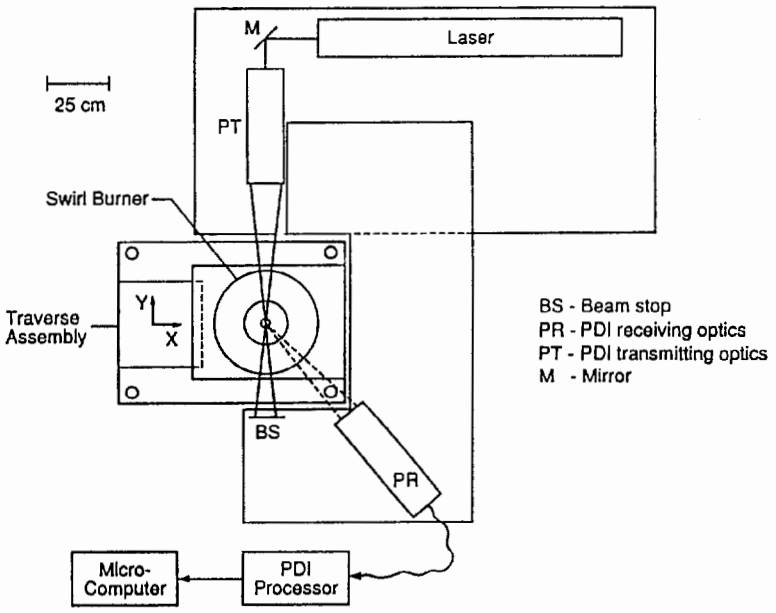

Fig. 3 Schematic of the experimental droplet size/velocity facility.

(see Fig. 4 of Ref. 4), and has a maximum value of approximately 2.3 m/s. The air velocities decay with increasing axial position. The tangential component of air velocity was also of the Rankine vortex type for these experimental conditions (the radial velocity component was negligible).

A two-channel phase Doppler interferometer[16] was used to obtain droplet size and velocity information on individual droplets passing through the measurement volume (see Fig. 3). The measurement technique employed is similar to a conventional dual-beam laser velocimeter, except that four detectors are located in the receiver assembly.[22] Measurement of the temporal frequency of scattered light from the probe volume interference fringe pattern is used to determine droplet velocity. Measurement of the spatial frequency of scattered light, obtained from two separated detectors, is used to infer the phase difference and to provide information on particle size. Mean properties were based on the statistical analysis of the ensemble sizes and velocities. The influence of droplet trajectory through the probe volume on inferred droplet size can lead to the measured droplet size distribution being broader than the actual size distribution within the spray.[23] The sensitivity of measured diameter to droplet trajectory is minimized by ensuring that the characteristic width of the probe volume is much greater than the particle diameter, and by measuring the scattered light intensity in the near-forward direction.[24] In the present setup, the scattering measurements were made in the near-forward direction (30-deg scattering angle) and the minimum probe volume width was on the order of 100 μm.

The phase Doppler system provides information on particle size between 1 μm and 300 μm with the optical arrangement employed in this investigation. The measurement volume is defined by the 119- and 113-μm laser beam waists at 514.5 and 488.0 nm, respectively (with a fringe spacing of approximately 6.6 μm for both laser beams). The focal lengths of the transmitting and receiving optics

were 495 and 500 mm, respectively. The focal length of the collimating lens was 300 mm. The receiving optics has a 100-μm slit. For the experiments carried out in this investigation, the photomultiplier detector voltages were optimized to provide the greatest sensitivity to the wide range of droplet sizes typically found in these sprays.[18] Near the spray boundary, which is defined as the location where the volume flux is largest in the swirling case, data acquisition rates were high (10,000 data points were collected within 120 s). In other regions of the spray, however, considerably more time was required to collect the same number of data points.

Near the spray boundary, the required system gain was significantly lower than near the spray centerline for the swirling case. The percent validation (i.e., percent difference between detected and validated signals) for the swirling case were at best as high as 75% and as low as 50%. For the nonswirling case, the percent validation reached a maximum of 80% and a minimum of 50%. The percent validation was not correlated to the spatial position. The effect of percent validation on number density and mass flux is discussed in more detail elsewhere.[4,5] Measurements were repeated at several selected positions to ensure measurement repeatability that was generally better than 5% near the spray boundary.

III. Results and Discussion

A. Droplet Mean Properties

Droplet mean properties (i.e., size, number density, and velocity) are presented to describe the global features of the kerosene spray. The effects of swirl on droplet transport are emphasized by comparing the spray under swirling conditions ($S = 0.53$) to the nonswirling case ($S = 0$). The effect of combustion on droplet transport is presented elsewhere.[25] The results for the nonswirling case were taken from an earlier investigation.[19] For a hollow-cone spray, it is reasonable to define the location of the spray boundary at the radial position where most of the fuel mass resides. This is accomplished by presenting the droplet volume flux, which is defined as the volume of the droplets passing a unit cross-sectional area per unit of time.[26] Thus, radial profiles of the volume flux are presented in Fig. 4 at axial locations z of 10, 25.4, 50.8, and 76.2 mm downstream of the nozzle exit. The solid boxes along the abscissa indicate the position of the burner passage walls, with the fuel nozzle located at the axis of the burner ($r = 0$). Coflowing air is introduced through the outer coaxial passage. The profiles in Fig. 4 (for both the nonswirling and swirling cases) indicate that radial positions exist at each axial position where the volume flux exhibits a maximum or peak and thus are used to define the spray boundary. The results show that the presence of swirl redistributes the droplets to much larger radial positions (by a factor of 2–3 at $z = 10$ mm) and the peaks are farther apart than in the nonswirling spray. The nonswirling case is indicative of the fuel mass distribution that results from the nozzle design. At $z = 10$ mm, the peak values for the nonswirling case are an order of magnitude higher than the swirling case (about 2×10^{-1} $cm^3s^{-1}cm^{-2}$ for $S = 0$ and 2×10^{-2} $cm^3s^{-1}cm^{-2}$ for $S = 0.53$). At $z = 76.2$ mm, the magnitude of both the nonswirling and swirling cases are of similar order (5×10^{-3} $cm^3s^{-1}cm^{-2}$ for $S = 0$ and 8×10^{-3} $cm^3s^{-1}cm^{-2}$ for $S = 0.53$). This result indicates that swirl promotes spray uniformity closer to the nozzle than in the nonswirling case where shear-induced drag disperses the droplets farther downstream.

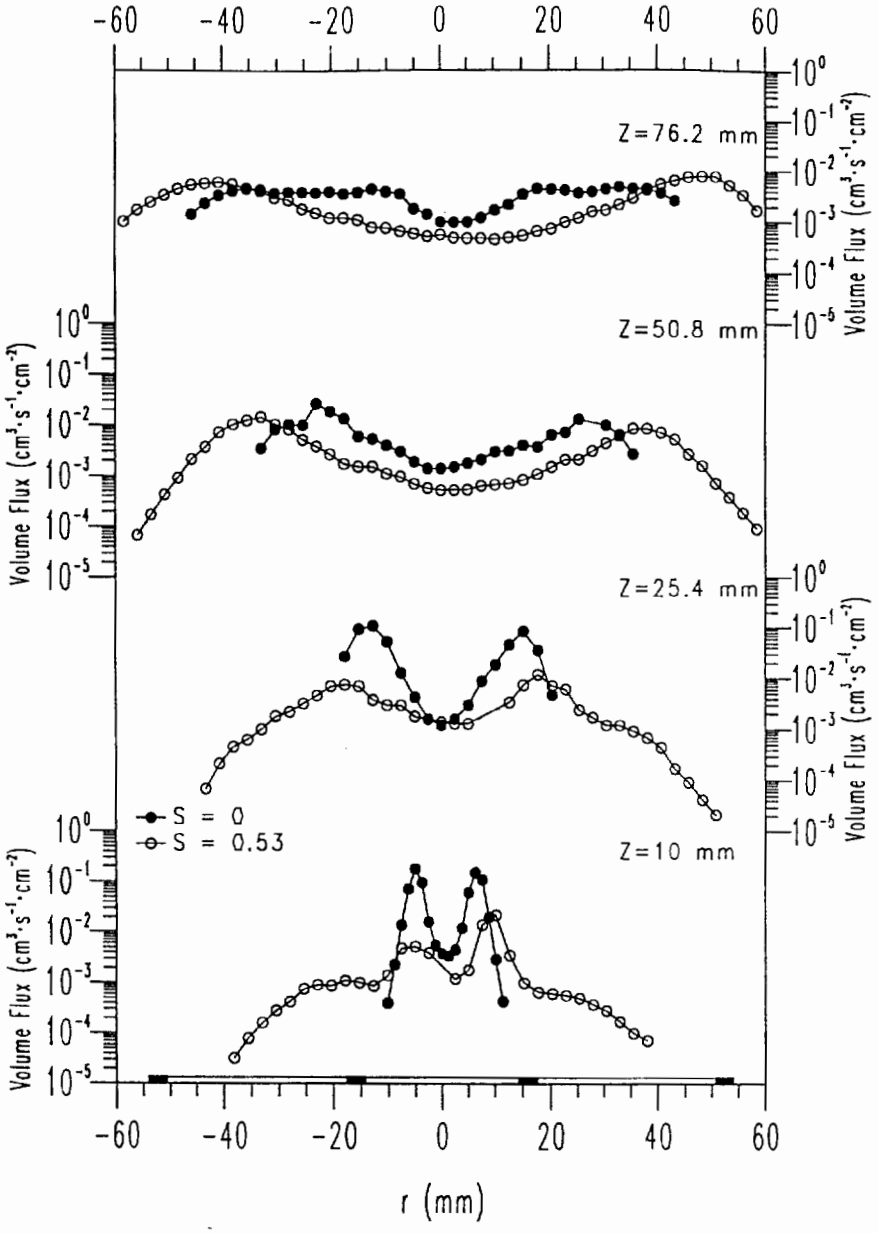

Fig. 4 Variation of volume flux with radial position r measured at different axial positions z for the nonswirling and swirling sprays.

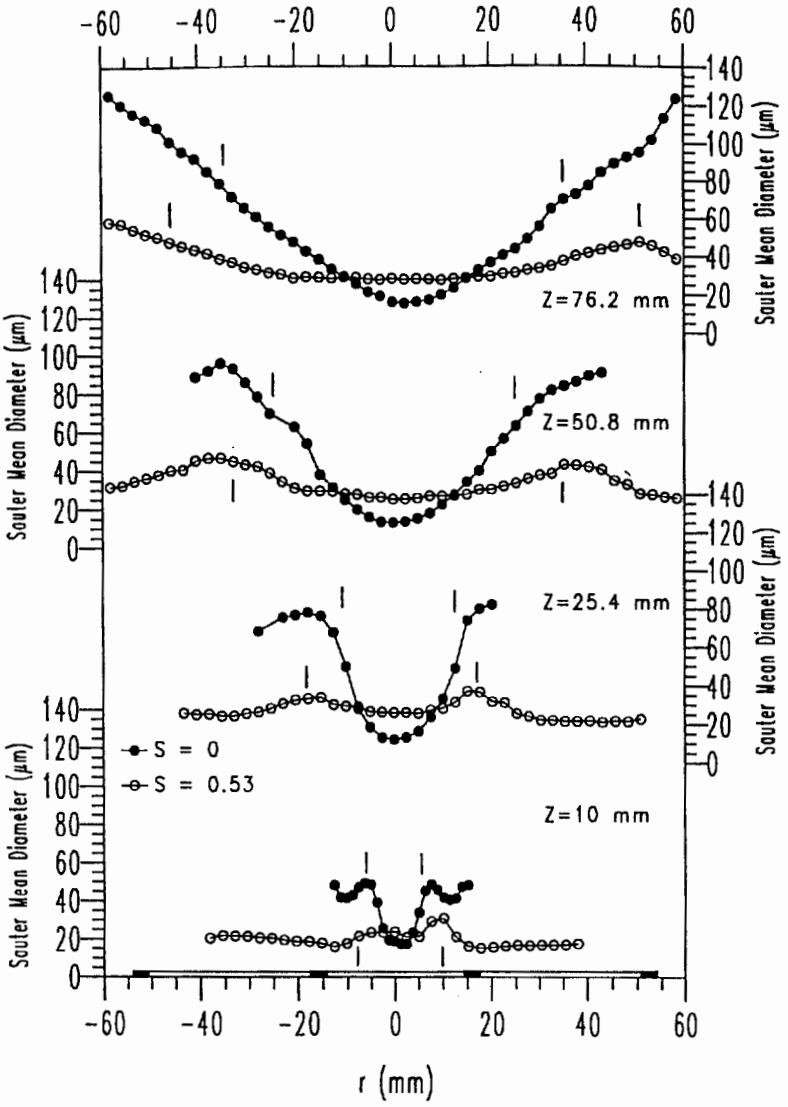

Fig. 5 Variation of Sauter mean diameter D_{32} with radial position r measured at different axial positions z for the nonswirling and swirling sprays.

Radial profiles of the droplet Sauter mean diameter D_{32} at the same four axial locations are presented in Fig. 5. The vertical bars identify the nominal spray boundary, which is defined as the radial location (at a given axial position) where the volume flux exhibits a peak (see Fig. 4). At each axial position, the spray boundary for the swirling case is located at a larger radial position than for the nonswirling case. The spray boundary also becomes ambiguous with increasing axial distance because of droplet dispersion. These peaks in Sauter mean diameter appear to match the peaks in volume flux for the swirling case at each axial position. For the nonswirling case, the peaks for D_{32} and volume flux are not

coincident at $z = 50.8$ mm and 76.2 mm because the droplet mean size increases monotonically with increasing radial position. Note again that the radial position of the peaks in volume flux are different for both cases, with the peaks for $S = 0$ being closer to the spray centerline than for $S = 0.53$. This difference is attributed to the centrifugal forces (present in the swirling case) displacing the bulk of the droplets radially outward from the spray centerline.

The profiles of Sauter mean diameter and volume flux for both cases indicate the expected broadening of the spray with increasing axial distance. The presence of relatively small droplets near the centerline and large ones near the spray boundary is attributed to the characteristic design of hollow-cone spray nozzles. Swirl, resulting in the formation of a toroidal recirculation region, increases the droplet radial dispersion (i.e., droplets were detected at larger radial positions) well beyond the radial position of the spray boundary. Without swirl, the values of D_{32} tend to increase monotonically with increasing radial position toward the edge of the spray at downstream axial positions. This result is attributed to the nozzle design in which the droplets are preferentially dispersed with the smaller droplets generally detected toward the spray centerline and larger droplets found at the largest radial positions. For the nonswirling case, there is also a gradual increase in the value of D_{32} along the spray boundary (from about 45 μm at $z = 10$ mm to 71 μm at $z = 76.2$ mm); see Fig. 5. This variation is attibuted to the shear layer mixing that occurs between the spray and the surrounding airstream, which results in radial dispersion of the smaller droplets. Another possible parameter to consider is some shear-enhanced vaporization of the smaller droplets.

Note also that the profile for the nonswirling spray at $z = 10$ mm exhibits a minimum in the value of D_{32} within the spray boundary. This is attributed to the fact that droplets at the periphery of the spray boundary (i.e., inner and outer surface of the hollow-cone spray structure) are in more direct contact with the surrounding airstream than those droplets within the spray boundary. The shear experienced at the spray periphery (both inner and outer surfaces) has a larger influence on the smaller droplets and disperses these droplets away from the boundary. Consequently, smaller droplets are less abundant at the spray periphery, which results in the formation of slight peaks for the droplet mean size.

The results presented in Fig. 5 indicate that the swirling spray has greater spatial uniformity and enhanced droplet mixing than for $S = 0$. As mentioned earlier, the nozzle is designed to disperse the larger droplets along the spray boundary and the smaller droplets near the spray centerline, which is apparent from the nonswirling spray results. Thus, in the swirling case, enhanced mixing would result in larger mean sizes near the center of the spray and smaller sizes toward the periphery. The weak radial variation of D_{32} for $S = 0.53$ (see Fig. 5) occurred at all of the measured axial positions, emphasizing the penetrating influence of swirl that is experienced by the surrounding airstream.

The variation of droplet mean size with axial position along the centerline and spray boundary is shown in Figs. 6a and 6b, respectively. Compared to the swirling case, the droplet mean diameter is smaller near the spray centerline (see Fig. 6a) and larger near the spray boundary (see Fig. 6b) in the nonswirling case. This feature results from the large variation in the droplet mean diameter for the nonswirling spray and the relatively small variation in mean diameter (greater spatial uniformity) for the swirling spray. The gradual increase in the values of D_{32} along the spray boundary (from approximately 31 μm at $z = 10$ mm to 48 μm at $z = 76.2$ mm for $S = 0.53$, see Fig. 6b) is again attributed to the

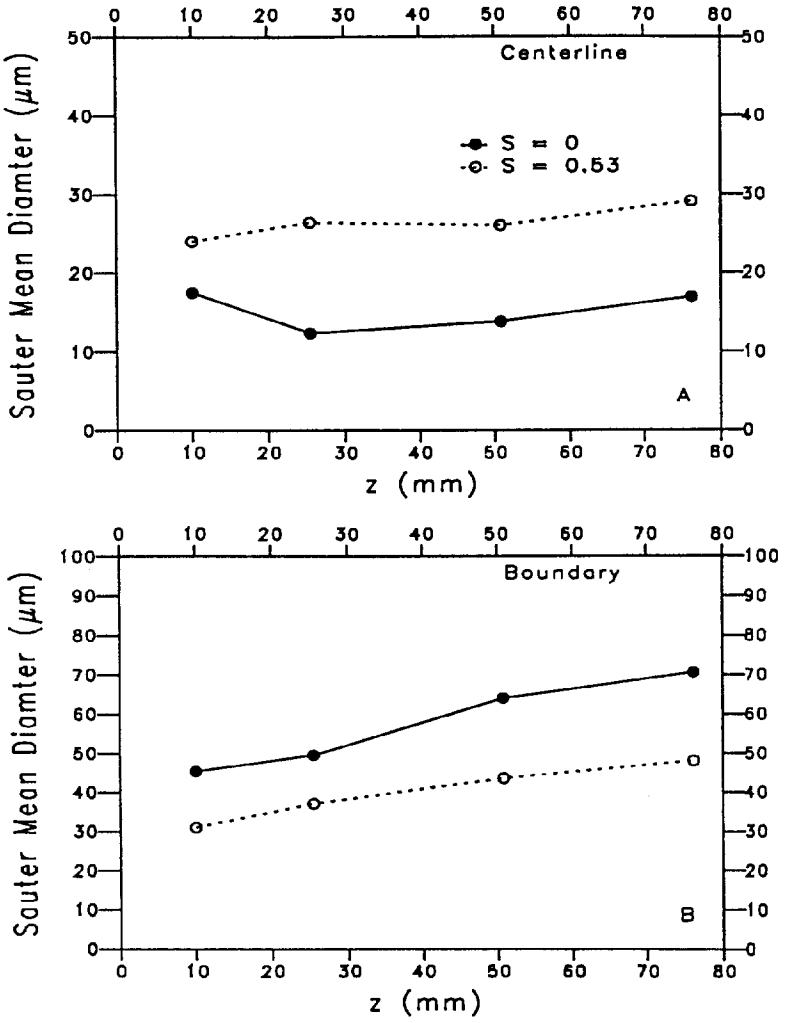

Fig. 6 Variation of Sauter mean diameter D_{32} with axial position along a) the centerline and b) the nominal spray boundary for the nonswirling and swirling sprays.

entrainment and transport of smaller droplets by the swirling flowfield; and the associated shear layer mixing that occurs between the spray and the surrounding airstream. This mixing promotes the depletion of smaller droplets in the spray boundary by means of such possible mechanisms as coalescence between droplets, droplet vaporization (both of which are expected to be insignificant due to the low probability of collisions between small droplets and the absence of combustion in this study), and radial dispersion away from the spray boundary. It is recognized, however, that the data obtained in this study cannot identify with certainty the precise mechanisms. The variation of droplet size with increasing axial and radial position is even more pronounced for $S = 0$ in which the values of D_{32} increase from about 45 μm at $z = 10$ mm to 71 μm at $z = 76.2$ mm (see Fig. 6b).

Near the spray centerline, there is little change in the value of D_{32} with increasing axial position for both cases (see Fig. 6a). For example, for $S = 0$ the change in the value of D_{32} is from 12 μm to 17 μm, and for $S = 0.53$ the change is from 24 μm to 29 μm. An increase in droplet mean size may be expected for the same reasons that there is an increase near the spray boundary. Elucidation of this transport phenomenon is made by examining the arithmetic mean diameter (D_{10}), which has a greater sensitivity to the smaller size droplets. The value of D_{10} increases slightly near the centerline for $S = 0.53$ from approximately 8 μm at $z = 10$ mm to 12 μm at $z = 76.2$ mm. This small variation in the values of D_{10} with axial position along the centerline is also small when $S = 0$. This small change may be explained by the lack of radial droplet dispersion in the nonswirling case, but would not describe the centrifugal effects on droplet transport along the spray centerline in the swirling spray. The small change in D_{10} for the swirling case may be attributed to the inward transport of smaller droplets by the toroidal recirculation zone, which replenishes the central region of the spray with smaller droplets from the spray periphery.

Results for droplet number density N for both the nonswirling and swirling sprays are presented in Fig. 7 for $z = 10$, 25.4, 50.8, and 76.2 mm downstream of the nozzle exit. The data indicate an increase in radial spread of the spray with axial position for both the swirling and nonswirling cases, with the swirling spray extending to much larger radial positions as compared to the nonswirling case. In the swirling spray, the maximum value of N occurred near the spray boundary where the larger droplets exist. In contrast, the maximum value of N for the nonswirling case is in the center of the spray despite the hollow-cone nature of the fuel nozzle. These profiles are indicative of the larger concentrations of relatively small droplets that remain confined to the center of the spray. The results for volume flux (see Fig. 4), however, indicate that the bulk of the mass does not reside near the spray centerline for $S = 0$. Based on the number density at $z = 10$ mm, there is no indication of the hollow-cone nature of the spray for which one would expect to find peaks in the values of N toward the spray boundary (see $z = 10$ mm in Fig. 8 of Ref. 4). This result may be attributed to the difficulty in detecting relatively small droplets (in the presence of larger ones) with the phase Doppler system because of the limited instrument dynamic range of 35:1; the spatial resolution was estimated to be sufficient because of the small probe volume size employed in this study.

The variation in number density with axial position is presented in Fig. 8 at both the centerline and spray boundary. The number density decreases as axial position increases for both cases. The values of N are larger for the nonswirling spray near the centerline but are significantly smaller toward the spray boundary. Near the centerline, the number density decreased slightly for $S = 0$ from $N \approx 9 \times 10^3$ particles/cm^3 at $z = 10$ mm to $N \approx 2 \times 10^3$ particles/cm^3 at $z = 76.2$ mm. For $S = 0.53$, number density changes from $N \approx 4 \times 10^3$ particles/cm^3 at $z = 10$ mm to $N \approx 1 \times 10^3$ particles/cm^3 at $z = 76.2$ mm. Near the spray boundary (as defined by the peaks in volume flux from Fig. 4, note vertical bars), the number density is similar to that near the centerline for $S = 0.53$ ($N \approx 5 \times 10^3$ particles/cm^3 at $z = 10$ mm to $N \approx 1 \times 10^3$ particles/cm^3 at $z = 76.2$ mm), but significantly lower for $S = 0$ at downstream positions ($N \approx 5 \times 10^3$ particles/cm^3 at $z = 10$ mm to $N \approx 6 \times 10^1$ particles/cm^3 at $z = 76.2$ mm). These differences between the nonswirling and swirling cases are attributed to the presence of significant air

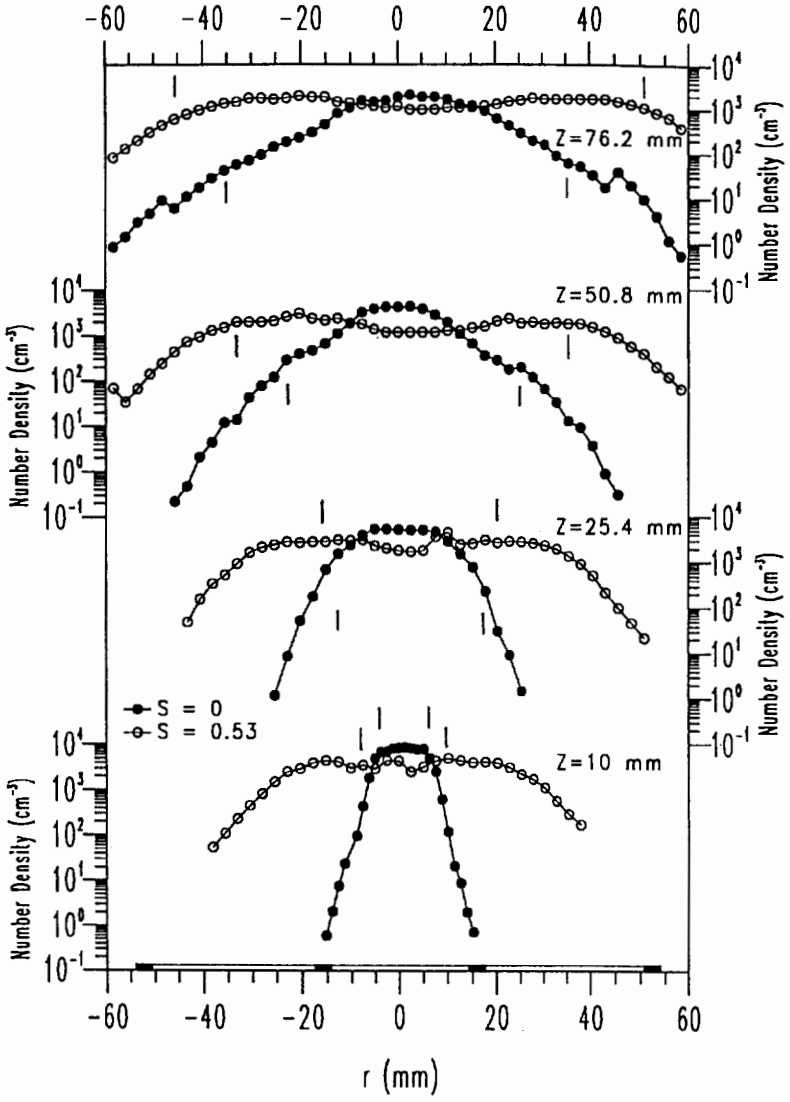

Fig. 7 Variation of number density N with radial position r measured at different axial positions z for the nonswirling and swirling sprays.

swirl in the latter case that promotes the radial dispersion and spatial uniformity of the fuel droplets.

The maximum values of N are significantly smaller than those measured with the polarization ratio technique[4] that is more sensitive to smaller size droplets. For these measurements, number densities were as high as $N \approx 1 \times 10^6$ particles/cm^3 in the upstream portion of the spray. This difference may be attributed to the lack of sensitivity of the phase Doppler system to detect submicron droplets, as well as other factors that lead to rejection of data (e.g., presence of multiple droplets

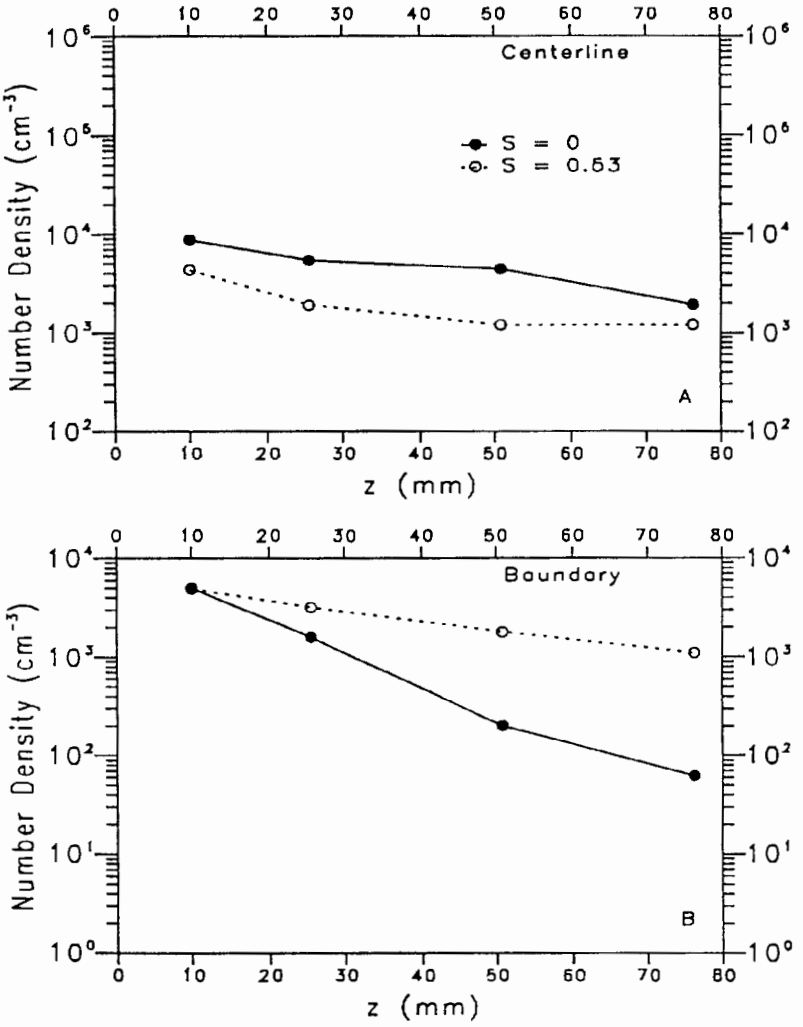

Fig. 8 Variation of number density N with axial position along a) the centerline and b) the nominal spray boundary for the nonswirling and swirling sprays.

in the measurement volume). Also note that for $S = 0$, the bulk of the mass does not reside in the center of the spray where transport of the smaller droplets occurs (see the volume flux in Fig. 4). The volume flux is larger near the spray boundary since it is proportional to $(D_{32})^3$ despite the smaller values of N. For $S = 0.53$ the mass resides near the spray boundary where both the size and number density are higher.

The spatial profiles of droplet mean axial u and radial v velocity components at $z = 10$, 25.4, 50.8, and 76.2 mm are shown in Figs. 9 and 10, respectively. Results for the swirling spray are again compared with those for the nonswirling spray.[19] Positive values of u correspond to droplets moving in the downstream direction

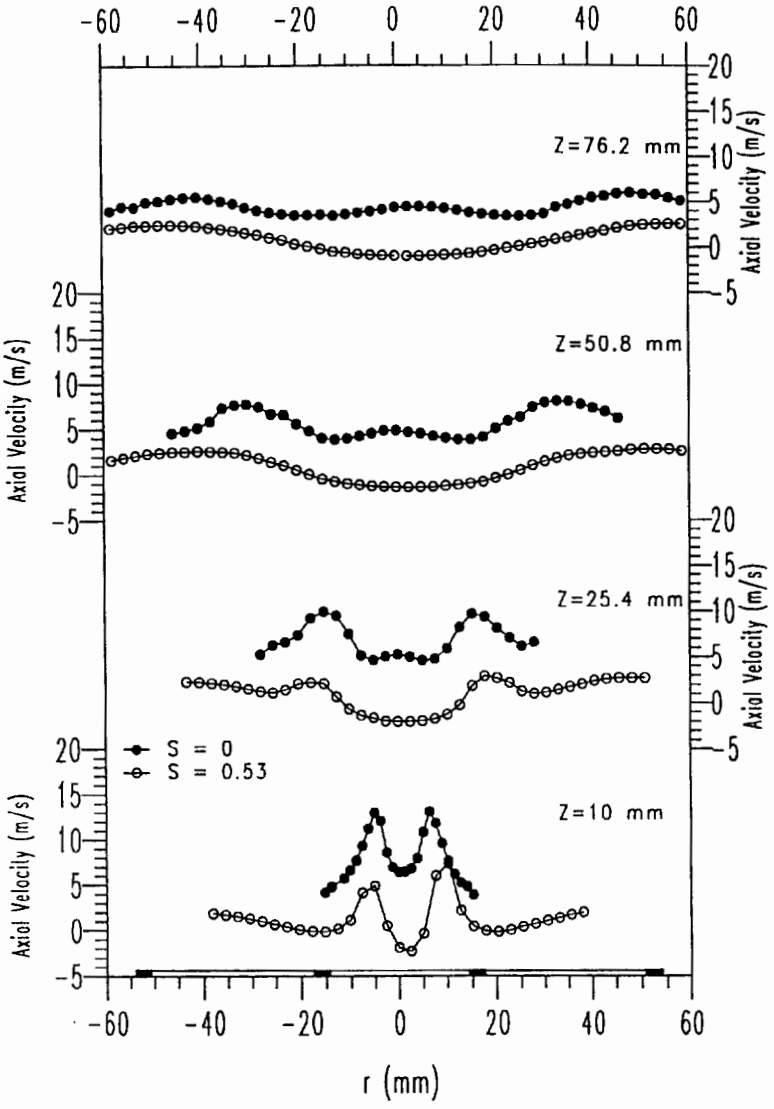

Fig. 9 Variation of axial velocity u with radial position r measured at different axial positions z for the nonswirling and swirling sprays.

(away from the atomizer) and positive values of v signify radially outward motion (that is, droplet motion away from the spray centerline). The results in Fig. 9 show that the magnitude of the droplet mean axial velocity decays with increasing axial position for both the nonswirling and swirling sprays. In contrast to the nonswirling spray, droplets in the swirling spray have negative axial velocities (and negligible radial velocities) at positions near the axis of the burner (see Fig. 9). These data indicate that droplet transport is upstream toward the fuel nozzle for the swirling spray.

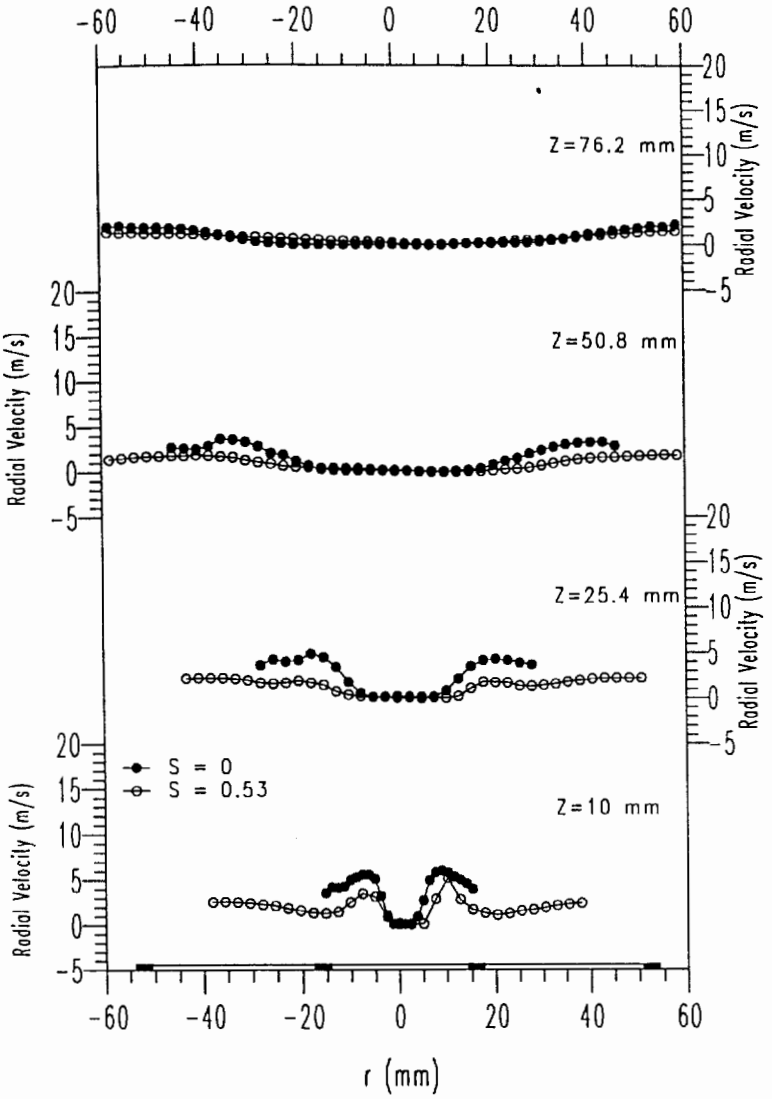

Fig. 10 Variation of radial velocity v with radial position r measured at different axial positions z for the nonswirling and swirling sprays.

The axial and radial velocity components of the droplets for the swirling and nonswirling sprays exhibit maxima near the spray boundary (see Figs. 9 and 10), with the mean flow corresponding to a direction that is consistent with the nominal spray cone half-angle (α in Fig. 11). When compared to the nonswirling case, the values of u and v are smaller for the swirling case since the centrifugal effects and droplet recirculation tend to diminish mean axial momentum and enhance spatial uniformity. For example, in the nonswirling case, given the peak values of $u \approx 13$ m/s and $v \approx 6$ m/s at $z = 10$ mm (as shown in Figs.

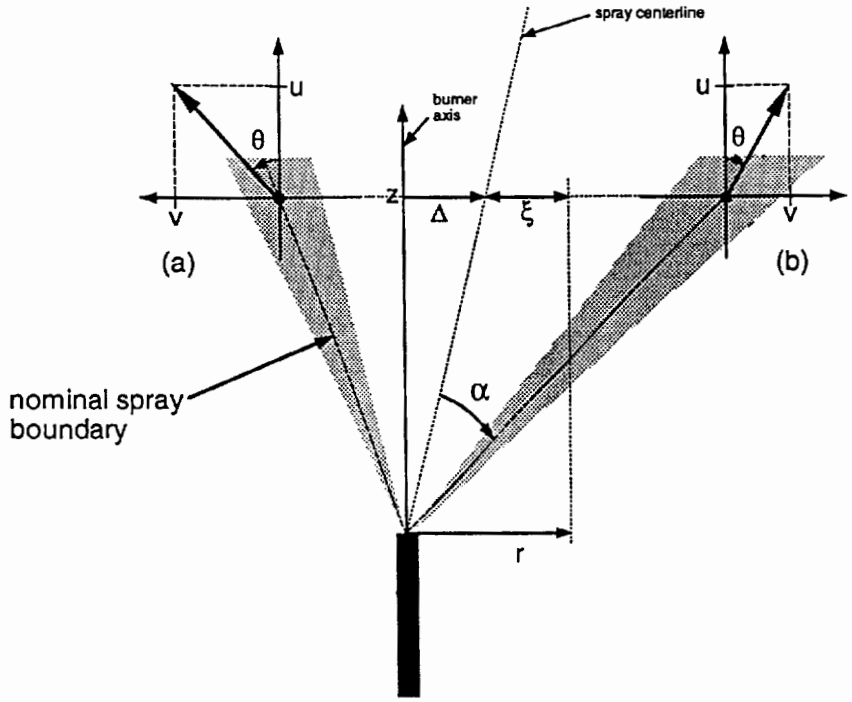

Fig. 11 Coordinate system used in the definition of droplet trajectory angle θ: coordinate a is replaced by b at the radial location where the magnitude of radial velocity component is a minimum ($\Delta = 0$ for a perfectly symmetric spray).

9 and 10), the mean flow direction θ of the droplets (see Fig. 11) is approximately 33 deg whereas the nominal spray angle α (as specified by the nozzle manufacturer) is about 30 deg. Near the spray boundary, the values of u for the nonswirling spray are at least a factor of two higher than those of the swirling spray (see Figs. 9 and 10); the values of v are similar near the spray centerline. Assuming that the droplet velocities at the nozzle are the same for both cases, this result suggests that the presence of swirl increases significantly the mean rate of droplet deceleration in the axial direction and increases the radial spread.

At $z = 10$ mm the respective rms values of the velocity components for both the nonswirling and swirling sprays indicate that the velocity distributions are narrower toward the spray centerline (i.e., smaller values of rms velocity) and wider toward the spray boundary (i.e., larger rms velocities) where the mean values reach a maximum. The spatial profiles of mean and rms velocity are similar at downstream positions of the spray, i.e., for $z \geq 50.8$ mm. To summarize, near the center of the spray, the droplet sizes are smaller and have a narrower velocity distribution (for both the axial and radial components). Toward the spray boundary, both the size and velocity distributions are wider.

B. Direction of Droplet Motion

The entrainment of droplets by the surrounding gaseous medium and secondary breakup of droplets in a spray are complicated phenomena involving aerodynamic drag forces and the creation of waves at the surface of droplets. Somewhat simplistic measures of these phenomena are provided by the Weber number ($=\bar{V}_{\text{rel}}^2 \rho D/\sigma$) for droplet breakup, the Stokes number ($=\rho_l D^2 \bar{V}_{\text{rel}}/18\mu\delta$) for dispersion and entrainment, and the Reynolds number ($=\bar{V}_{\text{rel}} D\rho/\mu$) for drag and internal circulation within droplets. In the definition of these parameters, $\bar{V}_{\text{rel}}$ is the relative velocity between the droplet and surrounding gas, ρ the gas density, ρ_l the liquid density, D the droplet diameter, σ the droplet surface tension, μ the gas phase viscosity, and δ a length scale characteristic of a vortex or eddy in the coflowing swirling gas stream. Two practical difficulties arise when evaluating these parameters for sprays. First, the droplet velocity relative to the surrounding gas phase is not easily obtained, and, second, the characteristic length scale for the recirculating vortex in the definition of the Stokes number is essentially unknown. Therefore, it would be inappropriate in this study to evaluate the Weber, Reynolds, and Stokes numbers. Information related to droplet transport, however, can still be obtained indirectly from the droplet velocity components.

The droplet velocity components were used to obtain a droplet mean trajectory angle θ, which is defined in Fig. 11. The symbol Δ is a measure of the asymmetry of the spray. The spray centerline is therefore defined to correspond to the radial position (at any axial location) where the radial velocity component is a minimum (see convention, defined earlier, for the velocity components). When $\Delta = 0$, the spray is symmetric about the axis of the atomizer. The value of Δ is determined at any axial location by first identifying the radial location at which the radial velocity component reaches a minimum. The symbol ξ is referenced to that location and $\xi = 0$ is the centerline. For $\xi > 0$, coordinate system b is used, and for $\xi < 0$ coordinate system a is used. With this choice of an axisymmetric coordinate system and sign convention for the velocity components mentioned earlier, negative values of θ will correspond to velocity vectors that are directed inward toward the centerline. For the conditions of the spray with swirl, the droplet tangential velocity component decays rapidly and becomes negligible within a few millimeters downstream of the nozzle.[4] Therefore, the u and v velocity components alone determine the direction of droplet motion in the two-dimensional (z–r) plane, where the droplet mean trajectory angle is $\theta = \tan^{-1}(v/u)$.

Variation of the droplet mean angle is presented in Fig. 12 at the various aforementioned locations within both the nonswirling and swirling sprays. In the outer radial regions of the spray, there is little difference in the direction of droplet motion between the two sprays at downstream positions (i.e., $z \geq 25.4$ mm), with the mean direction of droplet motion being in the nominal direction of the spray cone half-angle, which is about 30 deg. At $z = 10$ mm, however, there is a departure between the two cases. For $S = 0$, the spray cone angle (i.e., the trajectory angle near the edge of the spray) is preserved, namely, the mean droplet angle remains at approximately 30 deg. For $S = 0.53$, recirculated droplets are transported radially outward into the surrounding airstream and thus results in an increase in the mean angle (namely, the mean direction of motion is altered when considering the presence of the recirculated droplets in addition to the droplets that emanate from the nozzle). Near the spray centerline, droplets in the swirling

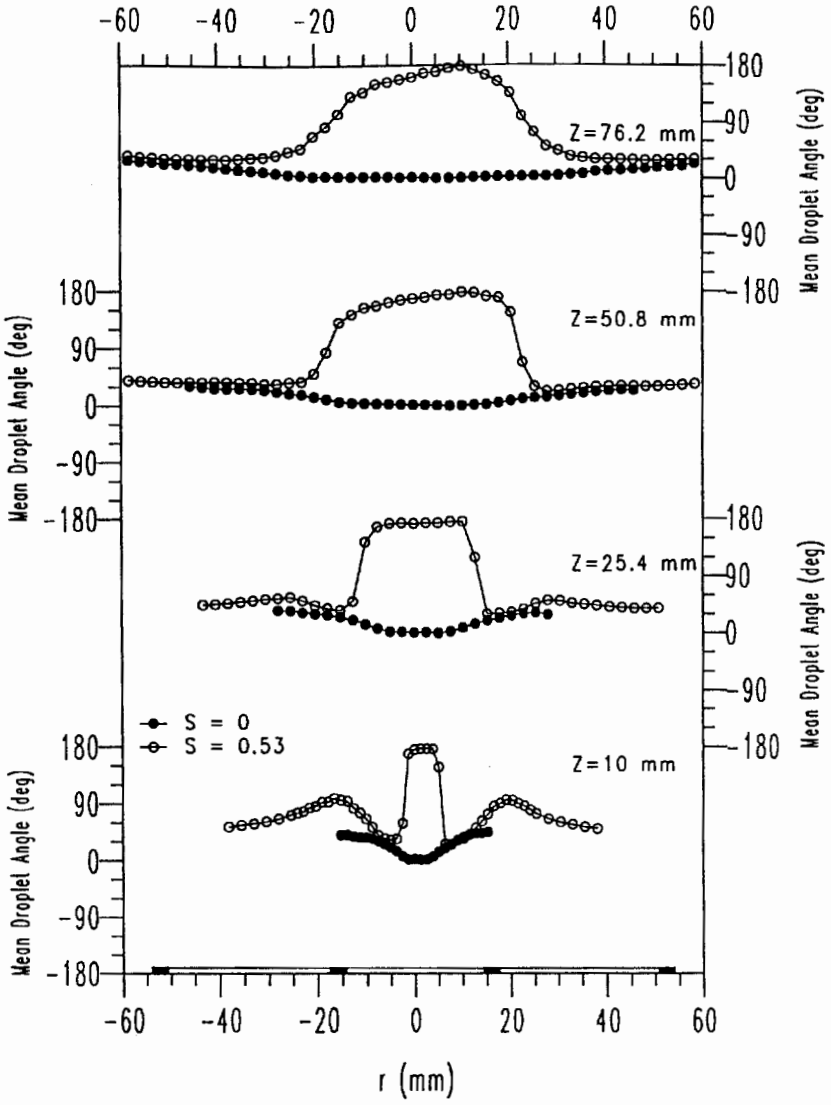

Fig. 12 Variation of droplet mean trajectory angle θ (see Fig. 10) with radial position r at different axial positions z for the nonswirling and swirling sprays.

spray move upstream in a direction opposite to those in the nonswirling spray (as a result of significant gas phase recirculation). For example, in the nonswirling spray $\theta \approx 0$ at the axis of the burner, whereas for the swirling spray $\theta \approx 180$ deg. Reasons for these differences in mean direction near the center of the spray are explored further by examining the size-classified distributions of droplet angle.

Distributions of droplet angle are presented in Figs. 13–15 at positions L1 ($r = 0$ mm), L2 ($r = 6.4$ mm), and L3 ($r = 10.2$ mm) from the centerline of the spray ($\Delta = 0$) to the spray boundary at $z = 10$ mm for both the nonswirling and swirling sprays. Since there is a slight asymmetry to the spray (e.g., see $z = 10$ mm

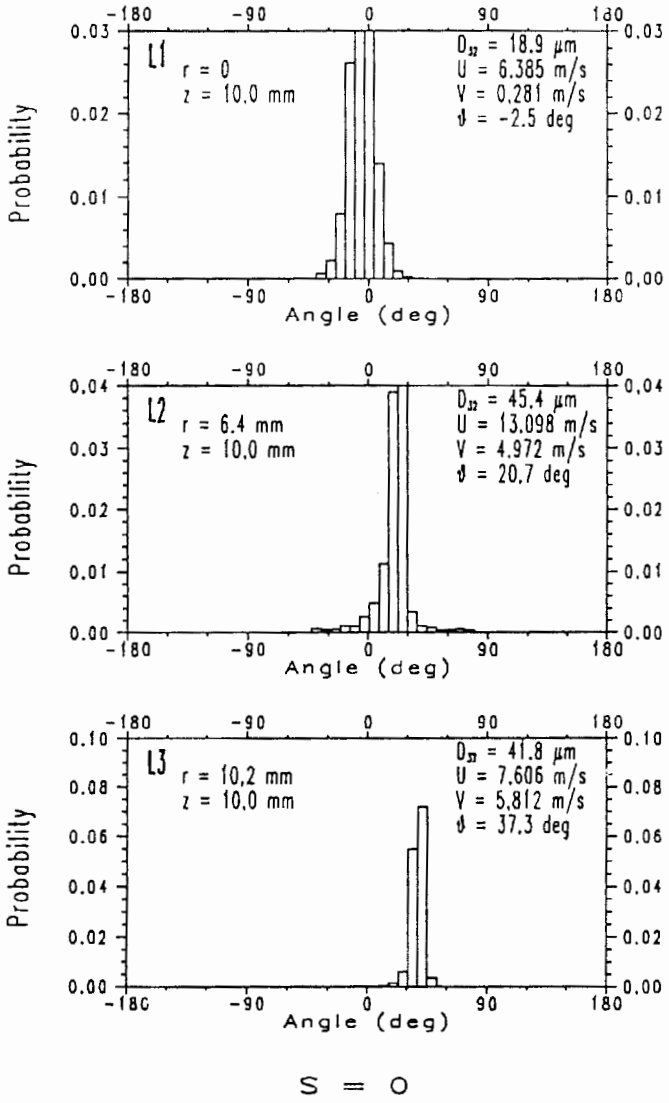

Fig. 13 Probability distributions (L1–L3) for droplet trajectory angles at three different locations in a nonswirling and swirling spray for all droplet sizes. ***(Continued)***

in Figs. 9 and 10), location L1 is positioned at $r = 0$ mm, $\Delta = 2.54$ mm, and $\xi < 0$ (i.e., $\xi = -2.54$ mm). The results presented in Fig. 13 show the distributions for all size classes, whereas the data in Figs. 14 and 15 are for specified size ranges: $1\ \mu m < D < 5\ \mu$m (hereafter referred to as 3-μm-size droplets) for Fig. 14, and $48\ \mu$m $< D < 52\ \mu$m (referred to as 50-μm-size droplets) for Fig. 15.

Differences between nonswirling and swirling conditions are evident from Fig. 13. In the swirling case, there is a wide distribution of angles (i.e., larger variance) at locations L1 and L2. This distribution becomes narrower (i.e., smaller variance) toward the spray boundary at L3. The wide distributions at locations L1

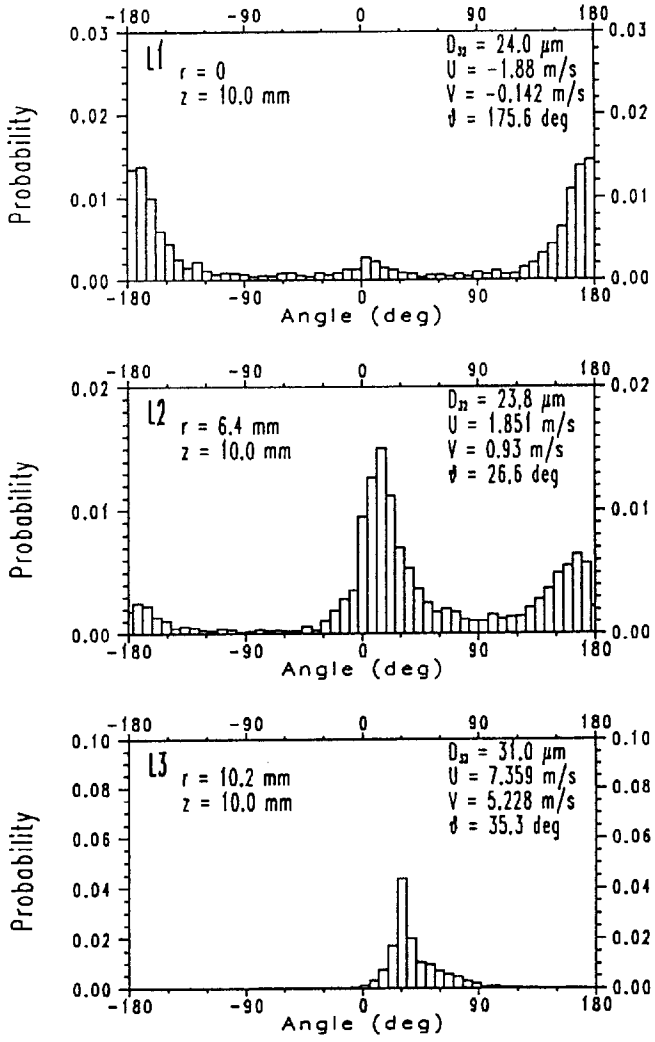

Fig. 13 *(Continued).*

and L2 for the swirling spray indicate the presence of two counter flowing streams, namely, droplets emanating directly from the nozzle (angle = ±90 deg) and recirculated droplets (±90 deg < angle < ±180 deg). In the nonswirling spray, all droplets are moving downstream away from the nozzle at each location, whereas in the swirling spray at L1, and to a lesser extent at L2, most droplets are moving upstream toward the nozzle. The fact that droplets tend to move in a ballistic fashion for the nonswirling spray has also been confirmed by laser sheet visualization of droplet trajectories in similar sprays.[4,27]

The size-classified angle distributions shown in Figs. 14 and 15 provide a more detailed depiction of individual droplet transport. Figure 14 shows that whereas the 3-μm-class droplets are generally moving in the downstream direction

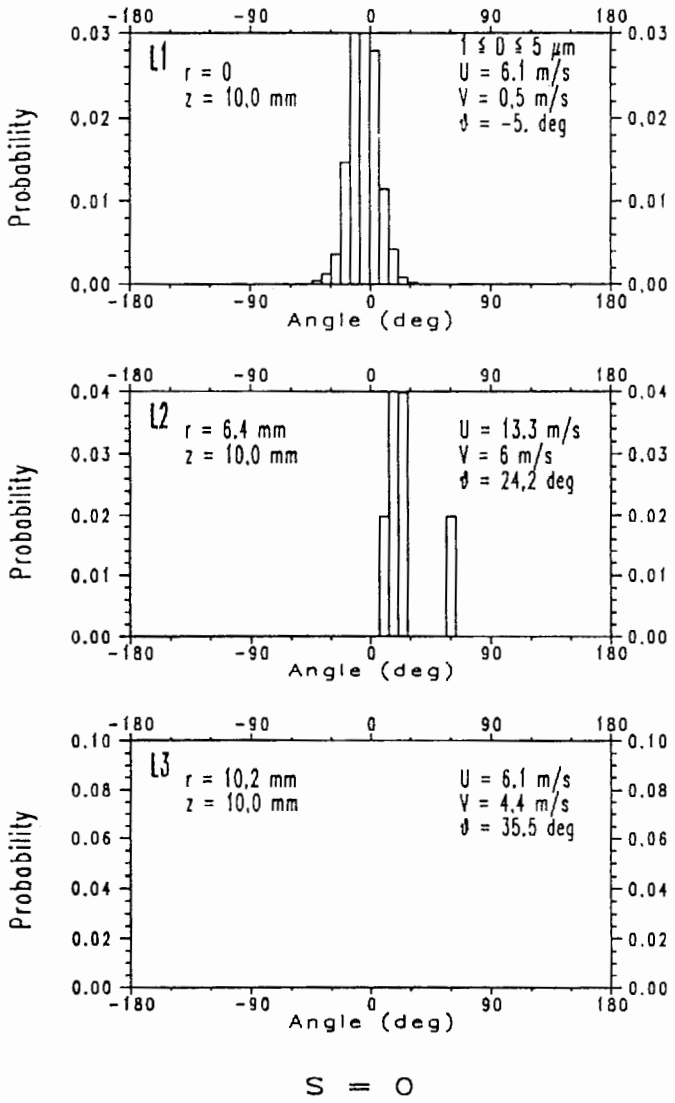

Fig. 14 Probability distributions (L1–L3) for droplet trajectory angles at three different locations in a nonswirling and swirling spray for droplets in the size range of 1–5 μm. ***(Continued)***

along the centerline (see frame L1) for the nonswirling spray ($\theta = -5.0$ deg), the range of directions is comparatively narrow. By contrast, in the swirling spray a significant number of 3-μm-size droplets are moving upstream at locations L1 and L2. This trend reflects the effect of recirculating gas phase motion on droplet relative velocity and drag. At location L3 (close to the spray boundary) for the swirling case, the few 3-μm-size droplets that were detected moved in the downstream direction. For the nonswirling case, 3-μm-size droplets were not detected at location L3 since the smaller droplets tend to be concentrated at the spray centerline for hollow-cone spray nozzles.

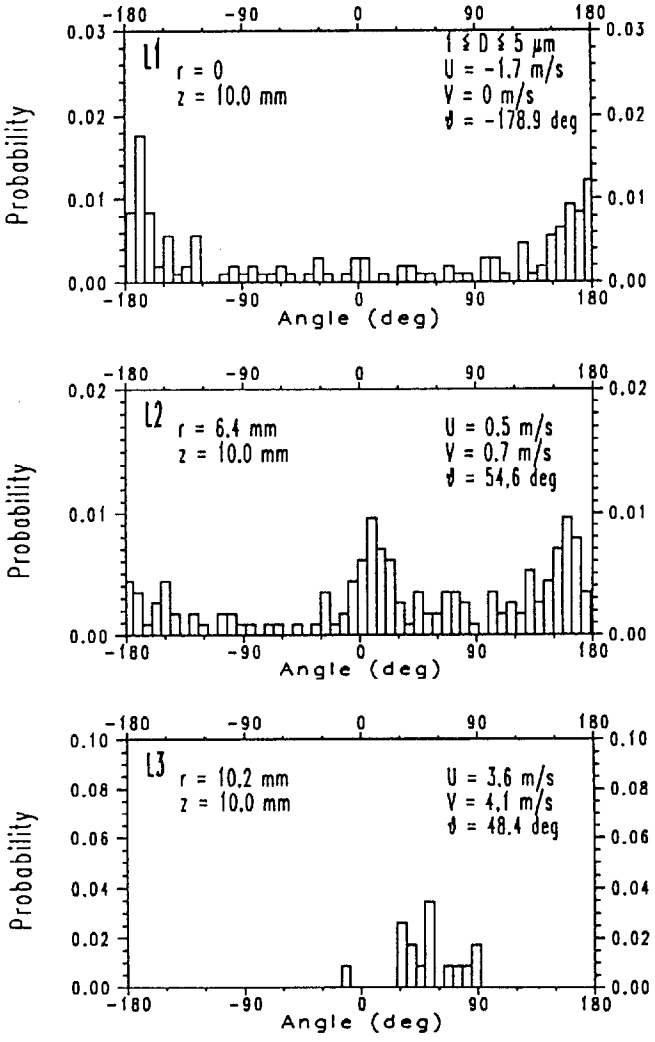

S = 0.53

Fig. 14 *(Continued).*

It is expected that smaller droplets will have a higher propensity to be carried along with the surrounding flowfield than the larger droplets that are relatively unaffected by the gas phase flow pattern. As shown in Fig. 15, 50-μm-size droplets in the nonswirling spray have a relatively narrow distribution of angles with only a few droplets deviating from the mean direction of droplet motion. Closer to the spray boundary (at locations L2 and L3) the droplet mean trajectory angle increases, from 20.5 deg at $r = 6.4$ mm to 36.8 deg at $r = 10.2$ mm at $z = 10$ mm. At location L1 (spray centerline), 50-μm-size droplets were not detected. The fact that larger droplets are not present at the center of the spray

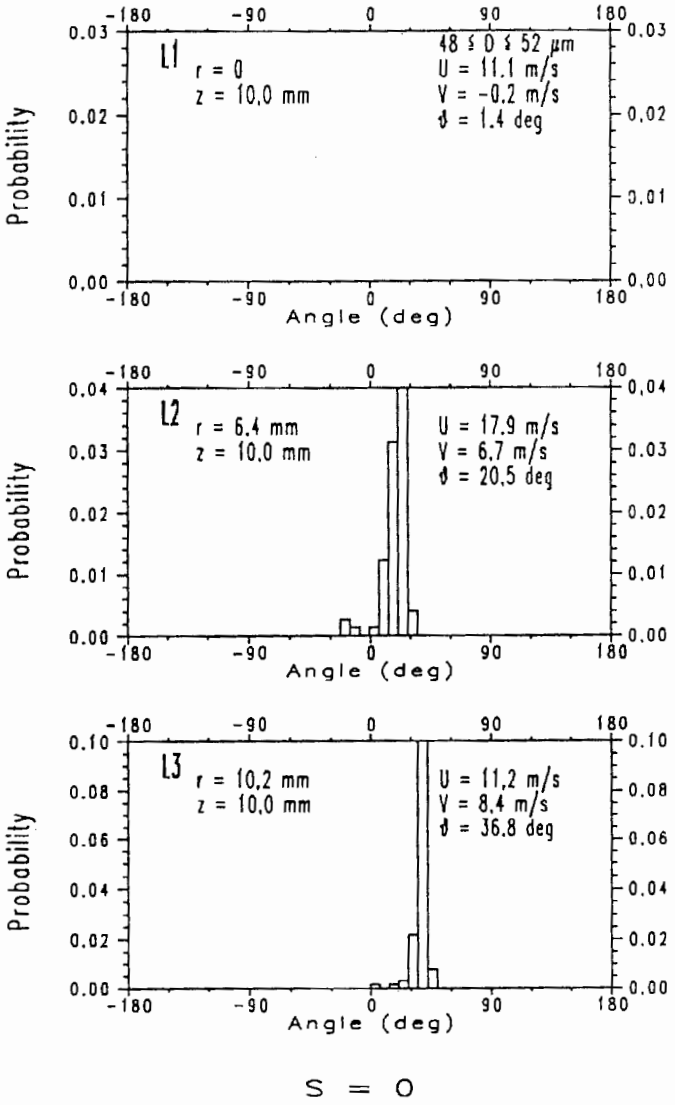

S = 0

Fig. 15 Probability distributions (L1–L3) for droplet trajectory angles at three different locations in a nonswirling and swirling spray for droplets in the size range of 48–52 μm. *(Continued)*

and smaller droplets are not found near the spray boundary is consistent with the hollow-cone nozzle design.

For the swirling spray, several 50-μm-size droplets are detected moving upstream as illustrated in Fig. 15 at locations L1 and L2. Such upstream motion of large droplets is surprising as it shows the comparatively strong entrainment of droplets by the surrounding air. Close to the spray boundary (at location L3), virtually all of the 50-μm-size droplets are moving in the direction of the nominal spray cone angle with no upstream droplet motion.

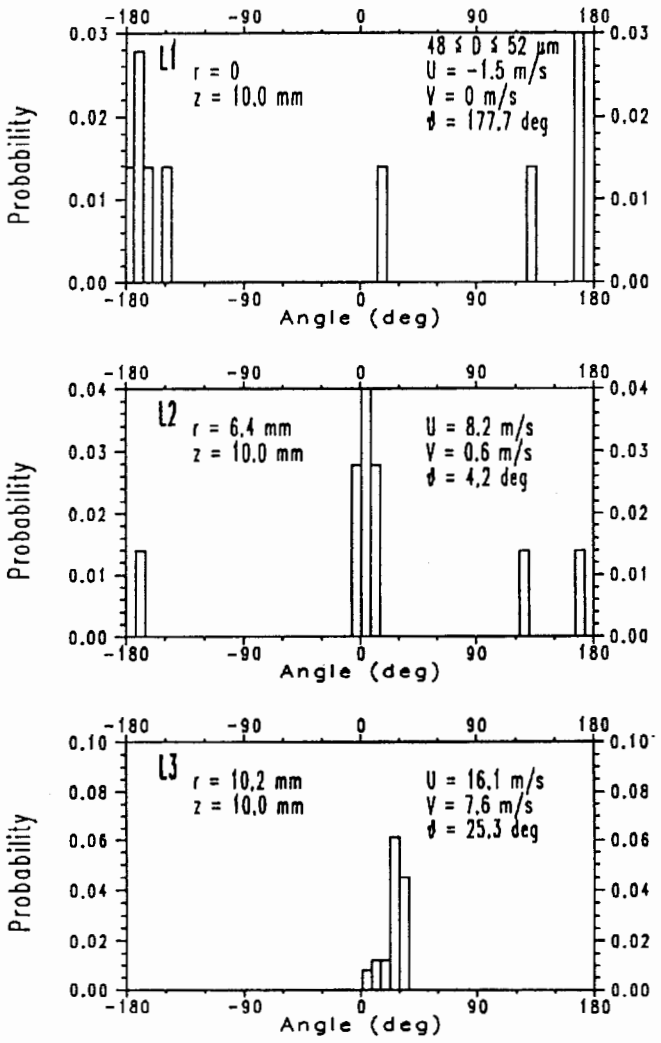

S = 0.53

Fig. 15 ***(Continued).***

C. Velocity and Droplet Size Correlation

The correlation among the droplet diameter and velocity components provides additional information relevant to understanding mechanisms of droplet transport in sprays. Figures 16 and 17 present such correlations at locations L1 and L3 under nonswirling and swirling conditions, respectively. The symbols in Figs. 16c, 16f, 17c, and 17f are coded to the droplet size as shown in the inset of Figs. 16f and 17f. At location L1 (burner centerline), the axial droplet velocity component is weakly correlated with diameter in both cases (i.e., weak linear dependence between diameter and axial velocity with a correlation coefficient r^2 of -0.2 for

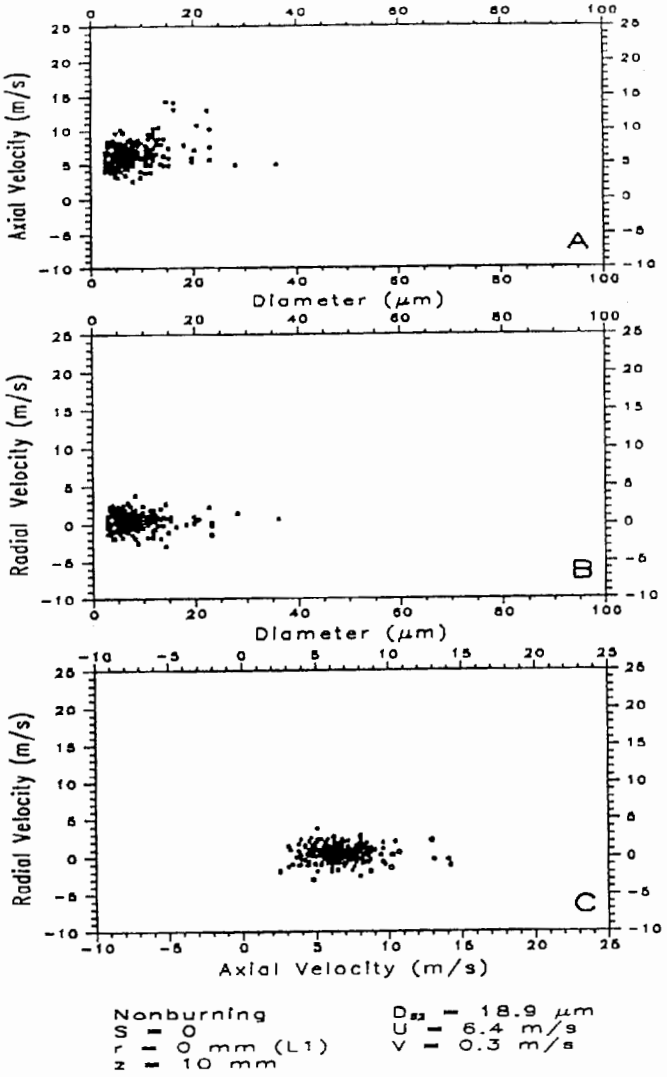

Fig. 16 Axial velocity/diameter, radial velocity/diameter, and axial/radial velocity correlations, respectively, at the centerline (location L1, frames a–c) and spray boundary (location L3 frames d–f) for the nonswirling spray; axial/radial velocity correlations are coded to represent the change in droplet diameter. ***(Continued)***

$S = 0$, and 0.5 for $S = 0.53$) as shown in Figs. 16a and 17a, though there is a slight increase in the values of u as diameter increases. Furthermore, for any given diameter, the axial velocity varies over a relatively large range. For example, the axial velocity of 10-μm-diameter droplets varies between about 3 m/s and 11 m/s for $S = 0$, and -5 m/s and 7 m/s for $S = 0.53$, as shown in Figs. 16a and 17a, respectively. By contrast, the radial velocity component is much smaller and shows much less scatter for a given droplet diameter than the axial component, as shown

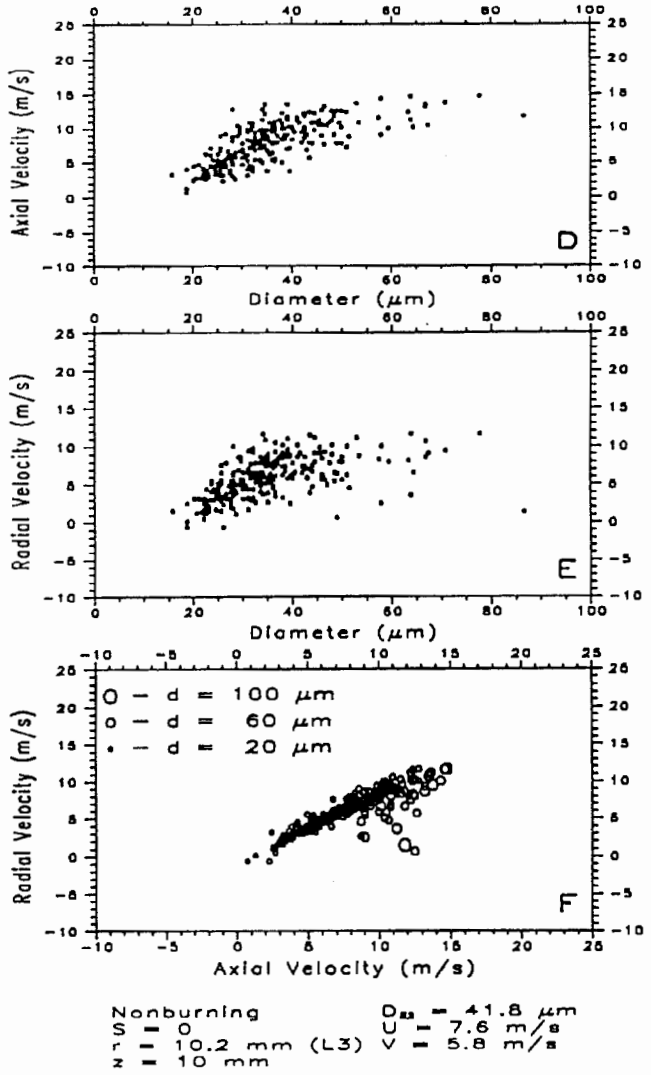

Fig. 16 *(Continued).*

in Figs. 16b and 17b (with the scatter decreasing as diameter increases). Figures 16c and 17c show the correlation between the two velocity components at location L1. The axial component is weakly dependent on the radial component, which is close to zero as shown in both Figs. 16c and 17c. The size-coded symbols in Figs. 16c and 17c show the tendency of larger droplets to have larger axial velocity components than smaller droplets. It is interesting to note that the effect of swirl near the centerline is to affect the velocity range (i.e., generate recirculated droplets), and that somewhat larger size droplets are present at the spray centerline than detected in the nonswirling case.

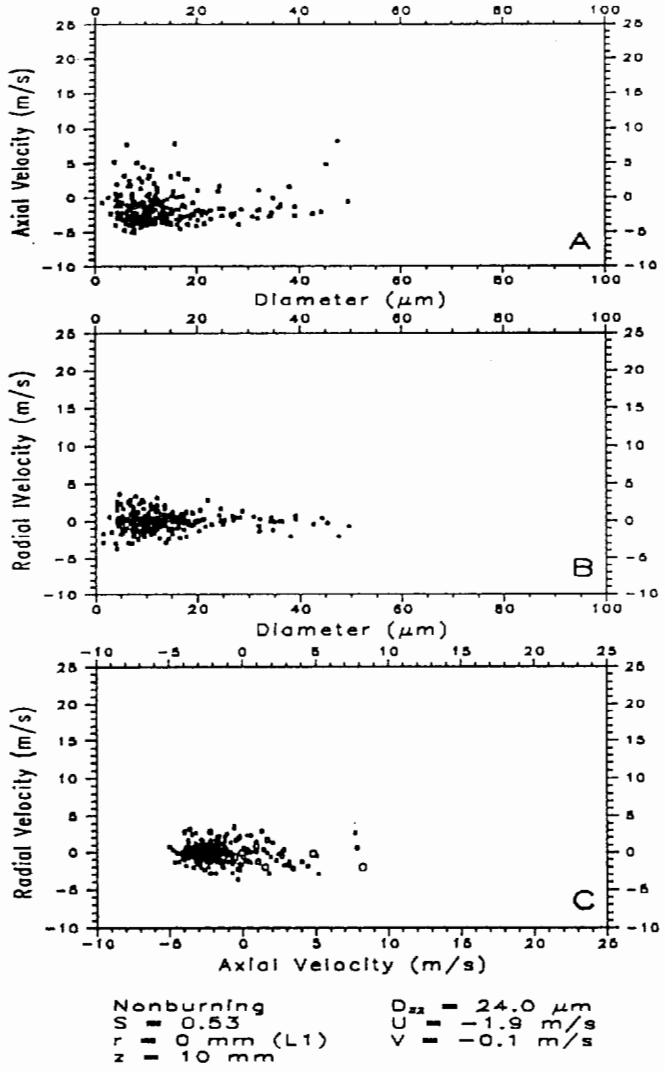

Fig. 17 Axial velocity/diameter, radial velocity/diameter, and axial/radial velocity correlations, respectively, at the centerline (location L1, frames a–c) and spray boundary (location L3 frames d–f) for the swirling spray; axial/radial velocity correlations are coded to represent the change in droplet diameter. ***(Continued)***

At location L3 (near the spray boundary, see Figs. 16d and 16e for $S = 0$ and Figs. 17d and 17e for $S = 0.53$) the results show a different trend than along the spray centerline. Whereas the axial velocity component does not vary strongly with droplet diameter at location L1 (see Figs. 16a and 17a), the correlation between axial velocity and diameter is more pronounced at location L3 ($r^2 \approx 0.7$ for $S = 0$ and $r^2 \approx 0.75$ for $S = 0.53$). For the nonswirling case, the value of u is well correlated with diameter over the range 5 μm $< D <$ 60 μm, whereas for

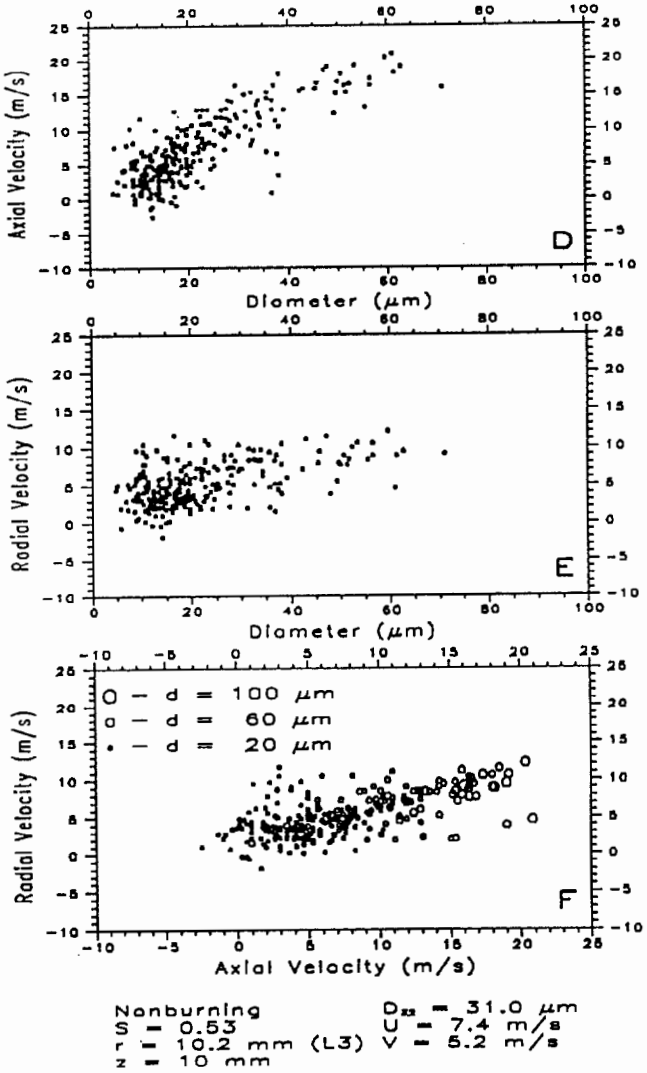

Fig. 17 *(Continued).*

$D > 60$ μm, the dependence of diameter on axial velocity appears to weaken sharply. For $D > 60$ μm, the radial velocity component also increases at a slower rate (with increased variance) and appears to approach an asymptotic value. Near the spray boundary, where the droplets are moving at comparatively higher velocity, a simple force balance on droplets shows that droplet deceleration is inversely proportional to diameter squared.[28] Since larger droplets will decelerate at a rate lower than that of the smaller droplets, the velocity of larger droplets is expected to be influenced less by droplet diameter than is the velocity of smaller droplets. For larger droplets, which would experience minimal deceleration, the droplet velocity should be independent of diameter in the spray (assuming that their initial

velocities at the nozzle exit are independent of diameter). This is consistent with the trends shown in Figs. 16d, 16e, 17d, and 17e.

The correlation between velocity components near the spray boundary shown in Figs. 16f and 17f is consistent with the mean trajectory angle shown in Fig. 12. Although these correlations are similar for both the swirling and nonswirling cases, there are some notable differences. The size-coded symbols in Figs. 16f and 17f again show the tendency of larger droplets to have larger axial velocity components than smaller droplets. The effect of swirl near the spray boundary is to affect the velocity range by widening the range of both the axial and radial velocity components as compared to the nonswirling case. This is again evident in Fig. 13 from the wider range of angles that is associated with the droplet motion in the swirling case.

IV. Summary

Droplet transport was examined in a kerosene spray using a phase Doppler interferometry system. The effect of swirl was studied by comparing a swirling spray to a nonswirling spray for the same operating conditions. For both the nonswirling and swirling cases, the larger droplets were found near the spray boundary and the smaller ones near the spray centerline, a characteristic of hollow-cone spray nozzles. Near the center of the spray, the size and velocity distributions are narrow, and there is little correlation between droplet size and velocity. Near the spray boundary, the width of the distributions are wider, and droplet size and velocity are better correlated near the nozzle exit. Near the nozzle exit, droplet momentum is far too large near the spray boundary for the surrounding turbulent airstream to have an influence on the droplets (including the smaller size droplets).

The presence of air swirl has several effects on droplet transport. Near the centerline, droplet transport is primarily upstream in the axial direction (i.e., reverse flow) as a result of the swirling air pattern. Under swirling conditions, the distribution of droplet trajectory angles is wider at each radial position across the spray than in the nonswirling case. This feature is most prominent near the spray centerline where a significant number of droplets (representing a wide range of droplet sizes) counterflow in the direction opposite to the droplets emanating directly from the nozzle. These results indicate that a moderate degree of swirl imparted to the airstream has a significant influence on individual droplet transport and on the overall spray structure.

Acknowledgments

The contributions of CTA were supported by the New York State Center for Hazardous Waste Management (A. Scott Weber, Director). The technical assistance of Michael J. Carrier and James D. Allen is greatly appreciated.

References

[1]Presser, C., Gupta, A. K., Avedisian, C. T., and Semerjian, H. G., "Fuel Property Effects on the Structure of Spray Flames," *Twenty-Third Symposium (International) on Combustion*, Combustion Inst., Pittsburgh, PA, 1990, pp. 1361–1367.

[2]Plee, S. L., and Mellor, A. M., "Flame Stabilization in Simplified Prevaporizing, Partially Vaporizing, and Conventional Gas Turbine Combustors," *Journal of Energy*, Vol. 2, No. 6, 1978, pp. 346–353.

[3]Rosfjord, T. J., and Russell, S., "Influences on Fuel Spray Circumferential Uniformity," AIAA Paper 87-2135, June 1987.

[4]Presser, C., Gupta, A. K., and Semerjian, H. G., "Aerodynamic Characteristics of Swirling Spray Flames: Pressure-Jet Atomizer," *Combustion and Flame,* Vol. 92, No. 1/2, 1993, pp. 25–44.

[5]McDonell, V. G., Cameron, C. D., and Samuelsen, G. S., "Symmetry Assessment of a Gas Turbine Air-Blast Atomizer," AIAA Paper 87-2136, June 1987.

[6]Mao, C. P., Wang, G., and Chigier, N., "An Experimental Study of Air-Blast Atomizer Spray Flames," *Twenty-First Symposium (International) on Combustion,* Combustion Inst., Pittsburgh, PA, 1986, pp. 665–673.

[7]Ghaffarpour, M., and Chehroudi, B., "Experiments on Spray Combustion in a Gas Turbine Model Combustor," *Combustion Science and Technology,* Vol. 92, Nos. 1–3, 1991, pp. 173–200.

[8]Bulzan, D. L., "Velocity and Drop Size Measurements in a Swirl-Stabilized, Combusting Spray," *SPIE—The International Society for Optical Engineering,* edited by L.C. Liou, Vol. 1862, 1993, pp. 113–122.

[9]Edwards, C. F., and Rudoff, R. C., "Structure of a Swirl-Stabilized Spray Flame by Imaging, Laser Doppler Velocimetry, and Phase Doppler Anemometry," *Twenty-Third Symposium (International) on Combustion,* Combustion Inst., Pittsburgh, 1990, pp. 1353–1359.

[10]Owen, F. K., "Measurements in Combustion System," *Laser Velocimetry and Particle Sizing,* edited by H. D. Thompson and W. H. Stevenson, Hemisphere, New York, 1978, pp. 123–135.

[11]Call, J. C., and Kennedy, I. M., "Particle Dispersion and Velocity Statistics in a Turbulent Shear Flow: Measurements and Simulations," *Proceeding of the Western States Section Meeting of the Combustion Institute* (Boulder, CO), Combustion Inst., Pittsburgh, PA, March 1991, Paper WWS/CI 91-38.

[12]Moreau, P., and Borghi, R., "Experimental and Theoretical Studies of Nitrogen Oxide Production in a Turbulent Premixed Flame," *Journal of Energy,* Vol. 5, No. 3, 1981, pp. 152–157.

[13]Crowe, C. T., Chung, J. N., and Troutt, T. R., "Particle Mixing in Free Shear Flows," *Progress in Energy and Combustion Science,* Vol. 14, No. 3, 1989, pp. 171–194.

[14]Uthuppan, J., Aggarwal, S. K., Grinstein, F. F., and Kailasanath, K., "Particle Dispersion in a Transitional Axisymmetric Jet: A Numerical Simulation," AIAA Paper 93-0105, 1993.

[15]Hardalupas, Y., Taylor, A. M. K. P., and Whitelaw, J. H., "Particle Dispersion in a Vertical Round Sudden-Expansion Flow," *Philosophical Transactions of the Royal Society of London A,* Vol. 341, No. 1662, 1992, pp. 411–442.

[16]Bachalo, W. D., and Rudoff, R. C., "Time-Resolved Measurements of Spray Drop Size and Velocity," *Liquid Particle Size Measurement Techniques: 2nd Volume,* ASTM STP 1083, edited by E. D. Hirleman, W. D. Bachalo, and P. G. Felton, American Society for Testing and Materials, Philadelphia, PA, 1990, pp. 209–224.

[17]McDonell, V. G., and Samuelsen, S., "Sensitivity Assessment of a Phase-Doppler Interferometer to User-Controlled Settings," *Liquid Particle Size Measurement Techniques: 2nd Volume,* ASTM STP 1083, edited by E. D. Hirleman, W. D. Bachalo, and P. G. Felton, American Society for Testing and Materials, Philadelphia, PA, 1990, pp. 170–189.

[18]Presser, C., Gupta, A. K., Avedisian, C. T., and Semerjian, H. G., "Effect of Dodecanol Content on the Combustion of Methanol Spray Flames," *Atomization and Sprays,* Vol. 4, No. 2, 1994, pp. 207–222.

[19]Presser, C., and Gupta, A. K., "Behavior of Droplets in Pressure-Atomized Fuel Sprays," AIAA Paper 93-0132, January 1993.

[21]Presser, C., Gupta, A. K., Semerjian, H. G., and Santoro, R. J., "Application of Laser Diagnostic Techniques for the Examination of Liquid Fuel Spray Structure," *Chemical Engineering Communications,* Vol. 90, April 1990, pp. 75–102.

[22]Gupta, A. K., Lilley, D. G., and Syred, N., *Swirl Flows,* Abacus, Kent, England, U.K., 1984.

[23]Bachalo, W. D., and Houser, M. J., "Phase/Doppler Spray Analyzer for Simultaneous Measurements of Drop Size and Velocity Distributions," *Optical Engineering,* Vol. 23, No. 5, 1984, pp. 583–590.

[24]Sankar, S. V., Buermann, D. H., Bachalo, W. D., and Robart, D. M., "Nonintrusive Characterization of Liquid-Liquid Mixing in Sprays," AIAA Paper 95-0138, 1995.

[25]Schaub, S. A., Alexander, D. R., and Barton, J. P., "Theoretical Analysis of the Effects of Particle Trajectory and Structural Resonances on the Performance of a Phase-Doppler Particle Analyzer," *Applied Optics,* Vol. 33, No. 3, 1994, pp. 473–483.

[26]Gupta, A. K., Presser, C., Hodges, J. T., and Avedisian, C. T., "The Role of Combustion on Droplet Transport in Pressure-Atomized Spray Flames," *Journal of Propulsion and Power,* Vol. 13, No. 3, May–June 1996.

[27]Zhu, J. Y., Rudoff, R. C., Bachalo, E. J., and Bachalo, W. D., "Number Density and Mass Flux Measurements Using the Phase Doppler Particle Analyzer in Reacting and Nonreacting Swirling Flows," AIAA Paper 93-0361, January 1993.

[28]Goix, P. J., Edwards, C. F., Cessou, A., Dunsky, C. M., and Stepowski, D., "Structure of a Methanol/Air Coaxial Reacting Spray Near the Stabilization Region," *Combustion and Flame,* Vol. 98, No. 3, 1994, pp. 205–219.

[29]Presser, C., Gupta, A. K., Hodges, J. T., and Avedisian, C. T., "Interpretation of Size-Classified Droplet Velocity Data in Swirling Spray Flames," AIAA Paper 95-0283, January 1995.